Experimental Study of the Higher $\pi \rightarrow \pi^*$ Transitions of Benzene in Low-Temperature Matrices

BENJAMIN KATZ
Department of Chemistry, Tel-Aviv University, Tel-Aviv, Israel
AND
MALKA BRITH
Department of Chemistry, Bar-Ilan University, Ramat-Gan, Israel
AND
BENJAMIN SHARF AND JOSHUA JORTNER
Department of Chemistry, Tel-Aviv University, Tel-Aviv, Israel

(Received 24 March 1969)

In this paper we present the results of an experimental study of the absorption spectrum of benzene and deuterated benzenes in solid Ar, Kr, Xe, and N_2 in the spectral region 2800–1700 Å, with special reference to the 2100- and to the 1850-Å transitions. Our main results are:

(a) On the basis of the observed vibrational structure the second excited singlet state of the benzene molecule is assigned to the $^1A_{1g} \rightarrow {}^1B_{1u}$ rather than to the $^1A_{1g} \rightarrow {}^1E_{2g}$ excitation.

(b) Theoretical calculations of the dynamic electronic–vibrational coupling between the $^1B_{1u}$ and the $^1E_{1u}$ states support the $^1B_{1u}$ assignment of the 2100-Å transition.

(c) The vibrational structure of the 1850-Å $^1A_{1g} \rightarrow {}^1E_{1u}$ transition was resolved.

(d) No experimental evidence for Jahn–Teller coupling in the $\pi \rightarrow \pi^*$ $^1E_{1u}$ state was observed, in agreement with theoretical analysis.

(e) Information on site splittings for the higher $\pi \rightarrow \pi^*$ excitation of benzene in rare-gas solids has accumulated.

(f) Analysis of matrix shifts for the $^1A_{1g} \rightarrow {}^1B_{1u}$ and $^1A_{1g} \rightarrow {}^1E_{1u}$ transitions indicates that the "solvent effect" is dominated by dispersion interactions.

(g) Information on deuteration effects on the $^1B_{1u}$ and $^1E_{1u}$ energy levels was obtained.

(h) Qualitative information on intramolecular radiationless decay in the two higher $\pi \rightarrow \pi^*$ excited states of the benzene molecule has been inferred from the linewidths in the absorption spectrum.

I. INTRODUCTION

The benzene molecule provides an important prototype for π-electron systems. The molecular electronic spectrum of benzene has served for many years as one of the attractive applications for theoretical calculations. Exhaustive experimental work was performed on the first electronic transition of benzene[1] (the 2600-Å system assigned to the $^1B_{2u}$ state) which has been studied in the vapor phase,[2] in hydrocarbon solutions[3] and low-temperature glasses,[4] in rare-gas solids,[5,6] and in the crystalline state.[7,8] In the first singlet excited state of the benzene molecule the line broadening arising from the occurrence of intramolecular radiationless transitions is negligibly small.[9–11] The experimental work by Paramenter and Kistiakowsky[12] indicates that the fluorescence quantum yield for the $^1B_{2u}$ state is about 0.3. Theoretical arguments[10,11] then imply that inhomogenous line broadening arising from intramolecular electronic relaxation is comparable to the radiative width. Thus the absorption lines for this transition in the gas phase are narrow (disregarding "trivial" broadening mechanisms[13–15] such as rotational effects). The most extensive information available for a complete analysis of the 2600-Å transition of benzene originates from studies of the vapor-phase spectra and from the utilization of zero-phonon lines (e.g., the Shpolskii effect)[16] of benzene in low-temperature hydrocarbon glasses. Additional information from the crystal spectra[7,8] and the spectrum in solid rare gases[5] relates to the observation of the crystal-field-induced pure electronic $^1A_g \rightarrow {}^1B_{2u}$ transitions which are symmetry forbidden in the isolated molecule.

Difficulties were encountered in the experimental studies and in the theoretical assignment of the higher excited $\pi \rightarrow \pi^*$ states of the benzene molecule.[1] Experimental studies of the second excited singlet state of this

[1] For a complete survey see G. Herzberg, *Electronic Spectra of Polyatomic Molecules* (D. Van Nostrand Co., Inc., Princeton, N.J., 1966), p. 555.
[2] (a) H. Sponer, J. Chem. Phys. **8**, 705 (1940); (b) H. Sponer, G. Nordheim, A. L. Sklar, and E. Teller, *ibid.* **7**, 207 (1939).
[3] J. R. Platt and H. B. Klevens, Chem. Rev. **41**, 301 (1947).
[4] S. Leach, R. Lopez-Delgado, and F. Delmas, J. Mol. Spectry. **7**, 304 (1962).
[5] Y. Daimant, R. M. Hexter, and O. Schnepp, J. Mol. Spectry. **18**, 158 (1965).
[6] R. B. Merrithew, C. V. Marusak, J. Mol. Spectry. **25**, 269 (1968).
[7] V. L. Broude, Usp. Fiz. Nauk **74**, 577 (1961) [Sov. Phys.—Usp. **4**, 584 (1962)].
[8] H. C. Wolf, *Solid State Physics*, F. Seitz and D. Turnbull, Eds. (Academic Press Inc., New York, 1959), Vol. 9, p. 1.
[9] G. W. Robinson, J. Chem. Phys. **47**, 1967 (1967).
[10] M. Bixon and J. Jortner, J. Chem. Phys. **48**, 715 (1968).
[11] M. Bixon and J. Jortner, J. Chem. Phys. **50**, 4061 (1969).
[12] G. B. Kistiakowsky and C. S. Paramenter, J. Chem. Phys. **42**, 2942 (1965).
[13] G. R. Hunt and I. G. Ross, J. Mol. Spectry. **9**, 50 (1962).
[14] J. P. Byrne and I. G. Ross, Can. J. Chem. **43**, 3253 (1965).
[15] J. H. Calloman, T. M. Dunn, and I. M. Mills, Phil. Trans. Roy. Soc. London **259A**, 499 (1966).
[16] E. V. Shpolskii, Usp. Fiz. Nauk **80**, 255 (1963) [Sov. Phys.—Usp. **6**, 411 (1963)].

system were performed in the gas phase,[17–21] in hydrocarbon solutions[3] and glasses,[22] and in the crystal.[23] This state is appreciably broadened due to the occurrence of radiationless decay.[10,11] In the room-temperature spectra the appearance of unresolved hot bands[15] also complicates matters. Low-temperature studies[22] of this transition in hydrocarbon glasses (3-methylpentane and isopentane which do not provide a proper Shpolskii matrix for the benzene molecule) and in rare-gas solids[23] led to some further information on the vibrational structure and matrix shifts for this transition. We have recently demonstrated[24] that the use of properly annealed host rare-gas matrix leads to a considerable reduction of the fine structure assigned to different trapping sites, thus facilitating the observation of this transition. From the theoretical point of view, it is well established that the second $\pi \rightarrow \pi^*$ singlet transition of the benzene molecule is symmetry forbidden.[1] The use of energy-levels calculation[25–29] could not resolve the question whether this level should be assigned to the $^1B_{1u}$ or to the $^1E_{2g}$ state. Both of these assignments have a long history. Recent semiempirical calculations by Bloor *et al.*[27] and by Keutecky[28] and further SCF MO CI calculations by Buenker *et al.*[29] seem to indicate that the $^1E_{2g}$ level is lower than the $^1B_{1u}$ state. The inclusion of double (and higher) excitations in the CI scheme has a pronounced effect on the $^1E_{2g}$ level making it the second most stable singlet excited state.[28,29] Theoretical calculations[30,31] of the vibronic induced intensity failed to resolve the assignment of the second level. An independent way to attack this problem involves the utilization of two-photon spectroscopy[32]; however, considerable experimental difficulties were not yet overcome.

The vibrational analysis of the third $\pi \rightarrow \pi^*$ transition in the gas phase is practically impossible, as this excited

TABLE I. Absorption spectrum of C_6H_6 in solid argon. Mixture deposited at 20°K and photographed at 20°K. $\delta\nu$ represents splittings between consecutive lines.

λ (Å)	ν (cm^{-1})	$\delta\nu$ (cm^{-1})	Intensity
2074	48 220		w
		230	
2064	48 450		s
		240	
2054	48 690		w
2038	49 070		w
		260	
2027	49 330		s
		250	
2017	49 580		w
1999	50 030		w
		250	
1989	50 280		s
		250	
1979	50 530		w
1963	50 940		w
		180	
1956	51 120		s
		270	
1946	51 380		w
1928	51 870		w
		240	
1919	52.110		s
		250	
1910	52 360		w
1854	53 940		w
		350	
1842	54 290		vs
		350	
1830	54 640		w
1823	54 850		w
		370	
1811	55 220		vs
		300	
1801	55 520		w
1790	55 870		w
		250	
1782	56 120		s
		310	
1792	56 430		w

TABLE II. Site splittings ($\delta\nu$) in the 2100-Å and 1850-Å transitions of benzene in inert matrices.

Molecule	Transition (Å)	Matrix	$\delta\nu$ (cm^{-1})
C_6H_6	2100	Ar	250±30
C_6D_6	2100	Kr	200±30
$C_6H_3D_3$	2100	Xe	250±30
C_6D_6	2100	N_2	150±30
C_6H_6	1850	Ar	350±30
C_6H_6	1850	Kr	300±30
C_6D_6	1850	Kr	210±30

[17] E. Carr and H. Stücklen, J. Chem. Phys. **6,** 645 (1938).
[18] W. C. Pryce and W. D. Walsh, Proc. Roy. Soc. (London) **A191,** 22 (1947).
[19] L. W. Pickett, M. Muntz, and E. M. McPherson, J. Am. Chem. Soc. **73,** 4862 (1951).
[20] J. Romand and B. Vodar, Compt. Rend. **223,** 930 (1951).
[21] M. Dunn and C. K. Ingold, Nature **176,** 55 (1955).
[22] W. J. Potts, Jr., J. Chem. Phys. **23,** 73 (1955).
[23] J. Y. Roncin, S. Y. Chen, J. Granier, and M. Damary-Astoin, Spectrochim. Acta **18,** 907 (1962).
[24] B. Katz, M. Brith, A. Ron, B. Sharf, and J. Jortner, Chem. Phys. Letters **2,** 189 (1968).
[25] R. G. Parr, D. P. Craig, and I. G. Ross, J. Chem. Phys. **18,** 1561 (1950).
[26] J. W. Moskowitz and M. P. Barnett, J. Chem. Phys. **39,** 1557 (1963).
[27] J. E. Bloor, J. Lee, and S. Gartside, Proc. Chem. Soc. **1960,** 413.
[28] J. Koutecky, *Modern Quantum Chemistry*—Istanbul Lectures, O. Sinanoğlu, Ed. (Academic Press Inc., New York, 1965), Vol. 1, p. 215.
[29] R. J. Buenker, J. L. Whitten, and J. D. Petke, J. Chem. Phys. **49,** 2261 (1968).
[30] J. N. Murrel and J. A. Pople, Proc. Phys. Soc. (London) **69A,** 245 (1956).
[31] A. C. Albrecht, J. Chem. Phys. **33,** 169 (1959).
[32] B. Honig, J. Jortner, and A. Szöke, J. Chem. Phys. **46,** 2714 (1967).

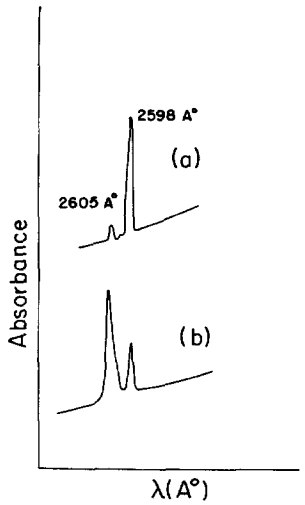

FIG. 1. Site splitting in the 2600 Å band of benzene in a krypton matrix. Upper curve: deposition at 40°K measurement at 20°K. Lower curve: deposition at 20°K measurement at 20°K.

state overlaps a Rydberg transition.[18,19,33] Potts observed vibrational structure for this transition in hydrocarbon glasses[22] and Roncin *et al.*[23] reported some further data on matrix shifts for this transition in solid rare gases. We have demonstrated[24] that the vibrational structure of this transition can be nicely resolved in annealed rare-gas solids. From the theoretical point of view, it is well established that the third singlet excited state corresponds to the $^1E_{1u}$ configuration.[1] This state may be subjected to Jahn–Teller coupling effects[34–44] which are not expected to be modified by the host matrix environment.

In this paper we present the results of an experimental study of the absorption spectrum of benzene and of deuterated benzenes in inert gas (Ar, Kr, Xe, and N_2) in the region 2800–1700 Å. A preliminary report of this work has already been presented.[24] The main results of our study can be summarized as follows:

(a) On the basis of the observed vibrational structure and intensity ratios of the vibrational components, the second excited singlet state is assigned to the $^1B_{1u}$ level. Theoretical results for the dynamic coupling between electronic and vibrational motion in the $^1B_{1u}$ state are consistent with the experimental data.

(b) Complete vibrational structure was resolved for the third ($^1E_{1u}$) singlet excited state. No evidence of Jahn–Teller coupling in this state was obtained, in agreement with theoretical semiquantitative evidence.

Some complementary information is also of interest:

(c) Qualitative information on site splittings in the $^1B_{1u}$ and $^1E_{1u}$ states of benzene in rare-gas solids was obtained. This information is complementary to that previously obtained for the $^1B_{2u}$ state.[5,6]

(d) Information on deuteration effects on the $^1B_{1u}$ and $^1E_{1u}$ energy levels is presented. These effects were extensively studied in the $^1B_{2u}$ state.[7]

(e) Information on matrix effects for the $^1A_{1g}\rightarrow{}^1B_{1u}$ and $^1A_{1g}\rightarrow{}^1E_{1u}$ transitions has accumulated.

(f) Qualitative information on the efficiency of intramolecular electronic relaxation in the $^1B_{1u}$ and in the $^1E_{1u}$ states is presented.

II. EXPERIMENTAL PROCEDURES

The gas mixtures were deposited on a cooled LiF window in the temperature range 4–45°K. The spectra were photographed at 4–20°K. The temperature-control device employed was described by Savitsky and Hornig.[45] Liquid hydrogen and liquid helium were used

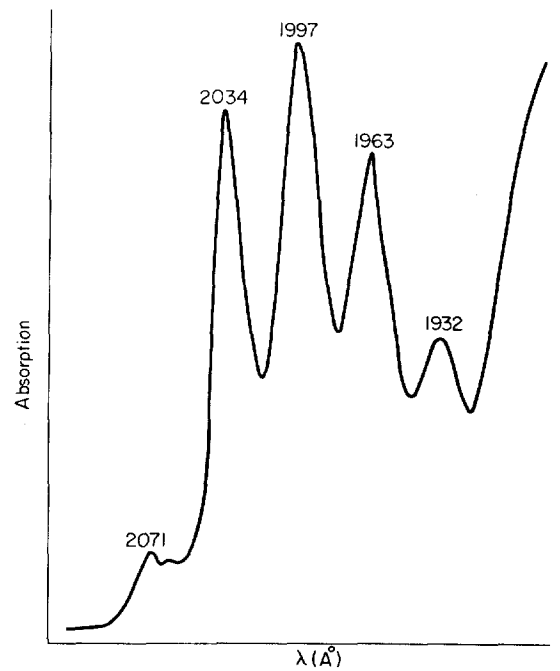

FIG. 2. The absorption spectrum of $C_6D_2H_4$ in a krypton matrix. The microdensitometer tracings are not corrected for variations in the source intensity. Mixture deposited at 40°K and spectrum photographed at 20°K. Numbers refer to wavelengths in angstrom units. The apparant band at 2060 Å is not real as it was not observed on the plates.

[33] P. G. Wilkinson, Can. J. Phys. **34**, 596 (1956).
[34] H. A. Jahn and E. Teller, Proc. Roy. Soc. (London) **A161**, 220 (1937).
[35] H. A. Jahn, Proc. Roy. Soc. (London) **A161**, 117 (1937).
[36] R. Renner, Z. Physik **92**, 938 (1934).
[37] H. C. Longuet-Higgins, U. Öpik, M. H. L. Pryce, and R. A. Sack, Proc. Roy. Soc. (London) **A244**, 1, (1958).
[38] W. E. Moffitt and H. D. Liehr, Phys. Rev. **106**, 1195 (1957).
[39] H. M. McConnel and A. D. McLachlan, J. Chem. Phys. **34**, 1 (1961).
[40] W. D. Hobey and H. D. McLachlan, J. Chem. Phys. **33**, 1694 (1960).
[41] W. D. Hobey, J. Chem. Phys. **43**, 2187 (1965).
[42] H. C. Longuet-Higgins, Advan. Spectry. **2**, 429 (1961).
[43] R. Fulton and M. Gouterman, J. Chem. Phys. **35**, 1059 (1961).
[44] A. Carrington, H. C. Longuet-Higgins, R. E. Moss, and P. F. Todd, Mol. Phys. **9**, 287 (1965).
[45] G. Savitsky and D. F. Hornig, J. Chem. Phys. **36**, 2634 (1962).

as refrigerants. The spectra were photographed on a 2-m Eagle mounting grating vacuum spectrograph[46] with a dispersion of 7.5 Å/mm in first order and a resolution of 50 000. Tanaka-type[47] Ar, Kr, and Xe light sources and a microwave dicharge H_2/D_2 source were used. Kodak SWR plates were employed. Microdensitometer tracings of the plates were prepared using a Joyce and Lable recording microdensitometer. In one case (Fig. 2) microdensitometer tracings were obtained using a Perkin–Elmer recording microdensitometer. The frequencies of the absorption bands were measured both from the microdensitometer tracings and directly from the plates. The emission lines of impurities of Hg, C, O, and H were used for calibration. In view of the appreciable line broadening in the second and third excited states of benzene all the measurements of the line frequencies are accurate within ± 30 cm^{-1}, while level spacings are accurate within ± 50 cm^{-1}.

The relative intensities of the bands corresponding to a single electronic transition were estimated by measuring the blackening of the plates with the aid of a point densitometer and interpolating the measured blackening units by the use of relative reference intensity units. The interpretation was carried out with the aid of a logarithmic step rotating disk. However, the calibration was performed on a Hilger spectrometer at $\lambda > 2000$ Å as it could not be done in the region of measurement as required for an accurate intensity calibration. The estimate of relative intensities of different vibrational components was carried out only for plates where the differences of blackening were not too high and where the absolute blackening was not too low. The accuracy of the relative intensities is estimated to be $\pm 30\%$.

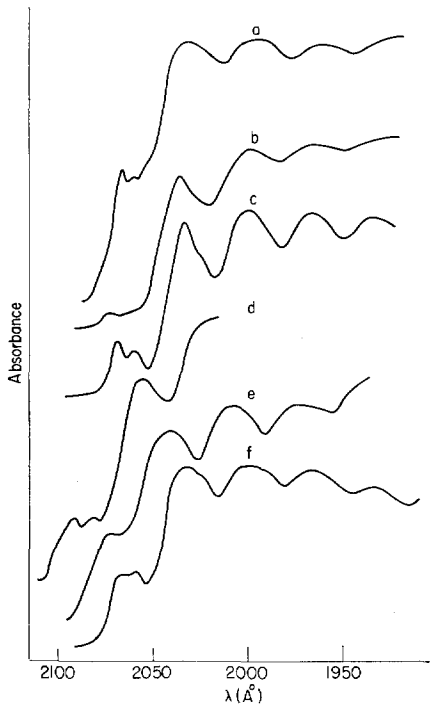

FIG. 3. The 2100 Å transition of benzene in inert matrices. The microdensitometer tracings were not corrected for the wavelength variations of the source intensity. (a) C_6H_6/Ar deposition and measurement at 20°K. (b) C_6H_6/Kr deposition at 40°K and measurement at 20°K. (c) C_6D_6/Kr deposition at 40°K and measurement at 20°K. (d) $C_6H_3D_3$/Xe deposition and measurement at 20°K. (e) C_6H_6/N_2 deposition and measurement at 20°K. (f) C_6D_6/N_2 deposition and measurement at 20°K. The tracings reveal pronounced fine structure in the two first vibrational components of Curves (a), (c), (d), and (f). Inspection of the plate shows that this fine structure prevails for all vibrational components.

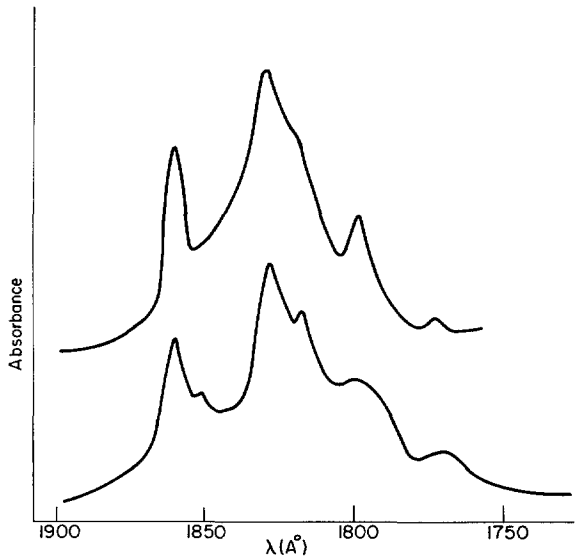

FIG. 4. The $^1A_{1g} \rightarrow {}^1E_{1u}$ transition of C_6H_6 in Kr (uncorrected microdensitometer tracings). Upper curve: deposition at 40°K measurement at 20°K. Lower curve: deposition and measurement at 20°K.

Benzene (Matheson) deuterated benzenes (Merck, Sharpe & Dohme) of spectrograde quality were used. The matrix materials were Ar, Kr, Xe (Linde and Matheson) and N_2 (Matheson) research grade. Mixture compositions of 1/50–1/500 were prepared before deposition. The thickness of the deposited samples varies from some tenths of a micron to several microns. On some special occasions much thicker samples were deposited.

III. SITE SPLITTINGS

The three $\pi \rightarrow \pi^*$ transitions of the benzene molecule located at 2600, 2100, and 1850 Å reveal a pronounced vibrational structure in the solid rare gases and in the N_2 matrix. Previous work[5,6] on the 2600-Å $^1B_{2u}$ state demonstrated the occurrence of different trapping sites in the matrix. We have found that deposition of C_6H_6 rare-gas mixtures at 20°K led to fine structure (see Table I) in the 2100- and in the 1850-Å transitions,

[46] M. Brith and O. Schnepp, Mol. Phys. 9, 473 (1965).
[47] Y. Tanaka, J. Opt. Soc. Am. 45, 710 (1955).

TABLE III. Vibrational features of the second and third $\pi \rightarrow \pi^*$ transitions of the benzene molecule in inert matrices at 20°K. ν corresponds to the peak position while $\Delta\nu$ is the separation between consecutive peaks. All energies are presented in cm^{-1} units. The location of vibrational peaks is accurate within ± 30 cm^{-1} while the separations are reliable within ± 50 cm^{-1}.

Compound	Matrix	ν (cm^{-1})	$\Delta\nu$ (cm^{-1})
A. 2100-Å transition			
C_6H_6	Kr	48 190	
			900
		49 090	
			910
		50 000	
			960
		50 960	
$C_6D_2H_4$	Kr	48 220	
			850
		49 070	
			930
		50 000	
			910
		50 910	
			900
		51 810	
$C_6D_4H_2$	Kr	48 280	
			870
		49 150	
			900
		50 050	
			900
		50 950	
			(800)
		(51 750)	
C_6D_5H	Kr	48 310	
			810
		49 120	
			860
		49 980	
			850
		50 830	
			840
		51 670	
C_6D_6	Kr	48 340	
			830
		49 170	
			850
		50 020	
			860
		50 880	
			870
		51 750	
C_6H_6	Ar	48 450	
			880
		49 330	
			950
		50 280	
			850
		51 130	
			970
		52 100	
$C_6D_3H_3$	Xe	47 840	
			840
		48 680	
			800
		49 480	
C_6H_6	N_2	48 190	
			870
		49 060	
			910
		49 970	
			890
		50 860	
			950
		51 810	
C_6D_6	N_2	48 470	
			840
		49 310	
			810
		50 120	
			840
		50 960	
			850
		51 810	
			870
		52 690	
B. 1850-Å transition			
C_6H_6	Kr	53 810	
			950
		54 760	
			920
		55 680	
			940
		56 620	
			950
		57 570	
$C_6D_2H_4$	Kr	53 870	
			900
		54 770	
			900
		55 670	
$C_6D_4H_2$	Kr	53 940	
			910
		54 850	
			890
		55 740	
C_6D_5H	Kr	53 970	
			880
		54 850	
			880
		55 730	
C_6D_6	Kr	54 000	
			850
		54 850	
			850
		55 690	
C_6H_6	Ar	54 290	
			930
		55 220	
			900
		56 120	
			930
		57 050	
			890
		57 940	
$C_6H_3D_3$	Xe	53 160	
			940
		54 110	
			900
		55 000	
			860
		55 860	
C_6H_6	N_2	53 880	
			930
		54 810	
			920
		55 730	
			940
		56 670	
C_6D_6	N_2	54 070	
			860
		54 930	
			870
		55 800	

which is assigned to site splittings. The site-splitting data are displayed in Table II. Our results for the $^1B_{2u}$ transition agree with the original work of Daimant, Hexter, and Schnepp.[5] The appearance of the fine structure in the 2600-Å transition was always observed simultaneously with fine structure in the 2100- and in the 1850-Å transition transition. Thus the appearance of fine structure in the 2600-Å transition could be applied as an adequate criterion for site splittings in the higher $\pi \rightarrow \pi^*$ transitions.

We have found that the deposition of the gaseous mixtures at different temperatures led to appreciable changes in the intensity ratio of the lines assigned to different trapping sites, while the positions of these lines were not altered. Deposition of C_6H_6–rare-gas mixtures at 40°K followed by measurements at 20°K led to an appreciable reduction in the fine structure assigned to different trapping sites. This behavior is demonstrated in Fig. 1 for the $^1A_{1g} \rightarrow {}^1B_{2u}$ $[0+\nu_{18}(e_{2g})]$ vibrational component (e.g., the false origin) of C_6H_6 in Kr. Thus, the high-temperature (40°K) deposition leads preferably to one trapping site. This pattern of behavior is observed simultaneously for all the three $\pi \rightarrow \pi^*$ transitions. In Fig. 2 we display the 2100-Å transition of $C_6D_2H_4$ in an annealed Krypton matrix, where the effect of site splitting is now considerably reduced.

The behavior of C_6D_6– and C_6D_5H–rare-gas matrices is appreciably different from that of C_6H_6–rare-gas matrices with respect to thermal annealing. The most detailed studies were performed on Krypton matrices. Deposition of C_6D_6/Kr and C_6D_5H/Kr mixtures at 40°K still led to appreciable fine structure due to site splitting with the two components being about the same intensity. This experimental observation should be viewed with some curiosity as the reason for the different behavior of C_6D_6 in inert matrices is obscure.

To summarize, the assignment of the fine structure in the three $\pi \rightarrow \pi^*$ transitions to different trapping sites is based on the following arguments:

(a) Different splittings were observed for the same transition in different matrices.

(b) The effect of thermal treatment for C_6H_6–rare-gas mixtures.

(c) The simultaneous appearance (or reduction) of the fine structure in the three transitions.

The experimental information obtained herein concerning site splittings makes it possible to approach confidently the interpretation of the molecular spectrum in the inert matrices.

IV. THE 2100-Å TRANSITION

The gross features of the 2100-Å transition of benzene and of deuterated benzenes in inert matrices are presented in Fig. 3. The lines are better resolved than in the room-temperature gas-phase spectrum in this region, mainly due to the removal of hot bands (and sequence congestion) in the low-temperature matrix. This effect is particularly significant for the first vibrational component which in the gas phase reveals a "splitting" of 150 cm^{-1}.[21] However, the matrix environment introduces new complications and the fine structure of the vibrational components which results from low-temperature (20°K) deposition of C_6H_6 and high-temperature (40°K) deposition of C_6D_6 is assigned to site splittings. In Table III we have summarized the vibrational structure characteristics of this transition (when site splitting is observed we refer only to the strong components), while the relative intensities of the vibrational components and the assignment are presented in Table IV. The observed features of the 2100-Å transition can be summarized as follows:

(a) Five broad lines are observed characterized by a spacing of 920±50 cm^{-1} in C H and 850±50 cm^{-1} for C D . Within this (rather poor) accuracy the vibrational spacings are independent of the host matrix.

(b) From the observed intensity pattern for the vibrational components (Table IV) it appears that in spite of the approximate equidistant spacing of all the five components the first weaker line does not correspond to the same vibrational progression as the others (see also Sec. X).

(c) The first vibronic component of this transition in the gas phase was reported[21] to reveal a doublet with a spacing of 150 cm^{-1}. In the low-temperature inert matrices only a single component is observed (the additional structure just arises from site splittings). Thus the low-energy component of the doublet reported by Dunn and Ingold[21] in the gas phase has to be attributed to a hot band. A reasonable assignment involves the 1–1 e_{2u} out-of-plane vibration which is characterized by a frequency of 404 cm^{-1} in the ground state and 240 cm^{-1} in the first excited singlet $^1B_{2u}$ state.[48]

TABLE IV. Relative intensities of the vibrational components in the $^1A_{1g} \rightarrow {}^1B_{1u}$ transition for C_6D_6 in Kr (accuracy of the intensity data ±30%).

ν (cm^{-1})	Relative intensity	Assignment[a]
48 340	1.0	$0\text{–}0+\nu_{18}(e_{2g})$
49 170	3.5	$0\text{–}0+\nu_{16}(e_{2g})$ and $0\text{–}0+\nu_{18}(e_{2g})+\nu_2(a_{1g})$
50 020	2.7	$0\text{–}0+\nu_{16}(e_{2g})+\nu_2(a_{1g})$ and $0\text{–}0+\nu_{18}(e_{2g})+2\nu_2(a_{1g})$
50 880	1.7	$0\text{–}0+\nu_{16}(e_{2g})+2\nu_2(a_{1g})$ and $0\text{–}0+\nu_{18}(e_{2g})+3\nu_2(a_{1g})$
51 750	0.7	$0\text{–}0+\nu_{16}(e_{2g})+3\nu_2(a_{1g})$ and $0\text{–}0+\nu_{18}(e_{2g})+4\nu_2(a_{1g})$

[a] The corresponding frequencies in the $^1B_{2u}$ state are as follows: $\nu_2(a_{1g})$ = 921 cm^{-1}, $\nu_{16}(e_{2g})$ = 1480 cm^{-1}, $\nu_{18}(e_{2g})$ = 521 cm^{-1} for C_6H_6 and $\nu_2(a_{1g})$ = 879 cm^{-1}, $\nu_{16}(e_{2g})$ = 1410 cm^{-1}, $\nu_{18}(e_{2g})$ = 499 cm^{-1} for C_6D_6 (see F. M. Garforth and C. K. Ingold, J. Chem. Soc. **1948**, 4170).

[48] F. M. Crawford, C. K. Ingold, and H. G. Poole, J. Chem. Soc. **1948**, 406.

TABLE V. Theoretical calculations of pseudo-Jahn–Teller coupling between the $^1B_{1u}$ and $^1E_{1u}$ states in the benzene molecule.

Source of input data and calculation method	K^{606} (cm^{-1})	K^{1174} (cm^{-1})	K^{1600} (cm^{-1})	Level spacings (cm^{-1}) relative to the lowest vibronic component[a] 1	2	3	Relative intensities 1	2	3
K terms estimated by Albrecht. Perturbation treatment (Ref. 31).	650	400	1500	0	568	989	1	0.38	5.3
K terms estimated by Albrecht (Ref. 31) Variational treatment (Ref. 52)	650	400	1500	0	650	900	1	0.69	0.19
K terms guessed to fit experimental data. Variational treatment (Ref. 52)	400	0	800	0	•••	835	1	0	3.1
Experiment (present work)	•••	•••	•••	0	Not observed	900±50	1	≪1	4.

[a] The lowest vibrational component refers to the first false origin built on the vibronic function which contains a major component of the $\nu_{18}(e_{2g})$ 606-cm^{-1} vibration.

(d) No experimental evidence could be obtained for the appearance of a (very weak) 0–0 line, which should appear on the low-energy side of the lowest vibronic component, and which could be induced by crystal-field interactions. We have looked for this line in thick samples (0.2 mm) without success. Thicker samples could not be utilized because of light scattering by the matrix and in view of the excessive line broadening in the first vibronic component. In partially deuterated benzenes vibronic coupling effects may lead to second-order mechanism for inducing the 0–0 line due to the reduction of vibrational symmetry. In thick (0.2-mm) samples of p-$C_6D_2H_4$ in Kr, a very weak line located $\sim$650 cm^{-1} to the red from the first vibronic component was observed. This very weak line in p-$C_6D_2H_4$/Kr could be tentatively assigned to vibronically induced 0–0 line which is further enhanced by crystal-field coupling. Unfortunately, this assignment is uncertain, as impurity effects cannot be ruled out and as we were unable to observe the weak 0–0 line in p-$C_6D_4H_2$/Kr samples.

Schnepp *et al.*[5] were able to identify the 0–0 crystal-field-induced pure electronic transition in the lower $^1A_{1g}\rightarrow{}^1B_{2u}$ excitation of benzene in thick rare-gas solids. Crystal-field mixing is known to be very efficient in the $^1B_{2u}$ state in crystalline benzene.[7,8] It is plausible that in a similar manner the pure electronic transitions to the second excited singlet state will be amenable to experimental observation in the benzene crystal.

On the basis of the experimental data we assign this transition to the $^1A_{1g}\rightarrow{}^1B_{1u}$ (rather than to the $^1A_{1g}\rightarrow{}^1E_{2g}$) excitation because of the following reasons:

(a) The observed vibrational structure and the relative intensities are consistent with this assignment. It is well known that the $^1A_{1g}\rightarrow{}^1B_{1u}$ transition is vibronically induced by vibrations of e_{2g} symmetry.[1,30,31] The carbon skeleton vibrations of this symmetry are $\nu_{18}(e_{2g})=521$ cm^{-1} and $\nu_{16}(e_{2g})=1480$ cm^{-1} for C_6H_6, where in the absence of better information we have utilized the available data for the $^1B_{2u}$ state. The first vibronic component in the 2100-Å transition is attributed to the false origin $0+\nu_{18}(e_{2g})$. The second line is assigned to the overlapping second false origin $0+\nu_{16}(e_{2g})$, and to the first totally symmetric vibration built on the first false origin $0+\nu_2(a_{1g})+\nu_{18}(e_{2g})$. Because of the excessive line broadening the two overlapping transitions constituting the second (and the higher) vibronic component cannot be resolved. It should be pointed out that the experimental spacing between the two first vibronic components, 920±50 cm^{-1} in C_6H_6 and 850±50 cm^{-1} in C_6D_6, while the differences between the frequencies of the two e_{2g} type vibrations are $\nu_{16}-\nu_{18}=1480-521$ $cm^{-1}=959$ cm^{-1} in C_6H_6 and $\nu_{16}-\nu_{18}=1403-499$ $cm^{-1}=904$ cm^{-1} in C_6D_6.

(b) The perturbation version of vibronic coupling Herzberg–Teller theory[30,31,49] indicates that the contribution of the "even" vibronic perturbation induced by the $\nu_{16}(e_{2g})=1520$-cm^{-1} skeleton vibration should be dominant for the $^1B_{1u}$ state.[30] The $^1B_{1u}$ state is subjected to pseudo-Jahn–Teller interactions with the $^1E_{1u}$ level and the simple perturbation treatment is not any more adequate[50–52] (see Sec. V). This problem will be discussed in the next section where we shall demonstrate that when a proper dynamic coupling scheme is considered, the effect induced by the "odd" perturbation due to the $\nu_{18}(e_{2g})$ vibration is appreciable. Semi-empirical choices of the vibronic coupling matrix elements indicate that the observed intensity ratio **1:4**

[49] G. Herzberg and E. Teller, Z. Physik. Chem. (Frankfurt) **B21,** 410 (1933).
[50] J. H. van der Waals, A. M. D. Berghius, and M. S. De Groot, Mol. Phys. **13,** 301 (1967).
[51] A. D. Liehr, Z. Naturforsch. **13a,** 596 (1958).
[52] B. Sharf, B. Honig, and J. Jortner, "Comments on the Vibronic Structure of Excited Electronic States," Mol. Phys. (to be published).

between the first and the second false origins in this transition is reasonable.

(c) This transition cannot be assigned to $^1A_{1g} \rightarrow {}^1E_{2g}$. The transition to the $^1E_{2g}$ state is expected to be induced by the $\nu_{14}(e_{1u})$ 1037-cm^{-1} and by the $\nu_{13}(e_{1u})$ vibrations with about equal efficiency.[30] Thus two false origins with a spacing of about 450 cm^{-1} are expected to be exhibited in the absorption spectrum.[53] This feature is not experimentally observed. Furthermore, the $^1E_{2g}$ state is expected to be subjected to Jahn–Teller coupling effects which will be manifested in the appearance of a progression of the nontotally symmetric e_{2g} vibration.[52] An analogous situation is encountered in the Rydberg states of benzene,[33] where the $\nu_{18}(e_{2g})$ progression appears. These features are not exhibited in the experimental spectrum. It should also be pointed out in this context that the argument of Dunn and Ingold[21] for the $^1E_{2g}$ assignment of the 2100-Å transition is not supported by our experimental results. From the experimental point of view the identification of a hot band on the low-energy side of the lowest vibronic component in the room-temperature gas-phase spectrum which does not appear in the low-temperature matrix provides a satisfactory interpretation for the doublet reported by Dunn and Ingold. On theoretical grounds[39] one can argue that the lowest vibronic component of a degenerate level should not split by Jahn–Teller interaction. The higher vibronic components are indeed split[39–43,52]; however, only the transition to one of the split components is allowed. Hence, one cannot assert that a doublet structure of a single vibronic component can provide evidence for Jahn–Teller interactions in a given electronic state.

V. PSEUDO-JAHN–TELLER COUPLING IN THE $^1B_{1u}$ STATE

It is well known that when two electronic states are closely spaced the conventional perturbation scheme for the Herzberg–Teller intensity-borrowing mechanism breaks down, and a more refined treatment based on the pseudo-Jahn–Teller effect has to be applied.[41–44,50,54] Such calculations for the $^1B_{1u}$ state coupled with the $^1E_{1u}$ state have been carried out by van der Waals *et al.*,[50] who argued that a single e_{2g} vibration dominates the vibronic mixing. Sharf *et al.*[52] have recently demonstrated that when one more vibration is involved in the coupling of two electronic states the validity criterion for the applicability of the first-order perturbation theory is $K^2/D\Delta\nu \ll 1$, where K is a typical vibronic coupling matrix element (due to one of these vibrations), D is the energy gap between the two electronic states, while $\Delta\nu$ corresponds to the difference in the frequencies of the two coupling vibrations. It may be thus concluded that when more than one vibration efficiently couples the two electronic states intravibrational coupling effects will seriously modify the level spacing and the absorption intensities.[52]

The proper treatment of the intensity borrowing in the $^1B_{1u}$ state of benzene should thus involve a dynamical treatment of the interaction between the electronic and nuclear motion, when several vibrations (of the same symmetry) couple the $^1B_{1u}$ and the $^1E_{1u}$ states. In what follows we shall present a brief review of a simple method[42,52] for generating vibronic wavefunctions and energies, which is based on the crude adiabatic approximation.[42] Consider two electronic states represented by the zero-order wavefunctions $\psi_n^0(\mathbf{q}, \mathbf{Q}_0)$ and $\psi_m^0(\mathbf{q}, \mathbf{Q}_0)$, where $\mathbf{q}$ corresponds to the electronic coordinates while $\mathbf{Q}_0 \equiv \{\mathbf{Q}_{i0}\}$ refers to the set of the nuclear coordinates $\mathbf{Q} \equiv \{\mathbf{Q}_i\}$ at a fixed configuration. The total molecular Hamiltonian is

$$H(\mathbf{q}, \mathbf{Q}) = T_e(\mathbf{q}) + T_N(\mathbf{Q}) + U(\mathbf{q}, \mathbf{Q}), \quad (1)$$

where the $T_e(\mathbf{q})$ and $T_N(\mathbf{Q})$ correspond to the electronic and nuclear kinetic-energy terms, respectively, and $U(\mathbf{q}, \mathbf{Q})$ represents the total potential-energy term. The zero-order wavefunctions referred to above are eigenfunctions of the electronic Hamiltonian at a fixed nuclear configuration

$$[T_e(\mathbf{q}) + U(\mathbf{q}, \mathbf{Q}_0) - E_n(\mathbf{Q}_0)]\psi_n^0(\mathbf{q}, \mathbf{Q}_0) = 0, \quad (2)$$

where $E_n(\mathbf{Q}_0)$ is the electronic energy at the fixed nuclear configuration.

A proper variational vibronic wavefunction is expanded in terms of the electronic wavefunctions:

$$\psi_p(\mathbf{q}, \mathbf{Q}) = \psi_m^0(\mathbf{q}, \mathbf{Q}_0)\chi_{mp}(\mathbf{Q}) + \psi_n^0(\mathbf{q}, \mathbf{Q}_0)\chi_{np}(\mathbf{Q}), \quad (3)$$

where only the contribution from closely lying electronic states has been taken into account. The expansion coefficients in Eq. (3) are then further expanded in terms of nuclear functions $N_i(\mathbf{Q})$ which are eigenfunctions of the nuclear equation in the ground electronic state which is characterized by the electronic energy $E_0(\mathbf{Q})$,

$$\{T_N(\mathbf{Q}) + \tfrac{1}{2}\sum_L [\partial^2 E_0(\mathbf{Q})/\partial Q_L^2]_0 Q_L^2 - W_N\} N_i(Q) = 0, \quad (4)$$

where a normal coordinate representation has been employed. The nuclear wavefunction corresponds to a product of harmonic-oscillator wavefunctions

$$N_i(\mathbf{Q}) = \prod_J |\, v_J\rangle, \quad (5)$$

where $|\, v_J\rangle$ refers to the harmonic nuclear function in the Jth normal mode in its v_Jth quantum state. So

[53] A dynamic Jahn–Teller calculation (Ref. 52) does not modify these qualitative considerations for the $^1E_{2g}$ state.

[54] M. Karplus, R. G. Lawler, and G. K. Fraenkel, J. Am. Chem. Soc. **87**, 520 (1965).

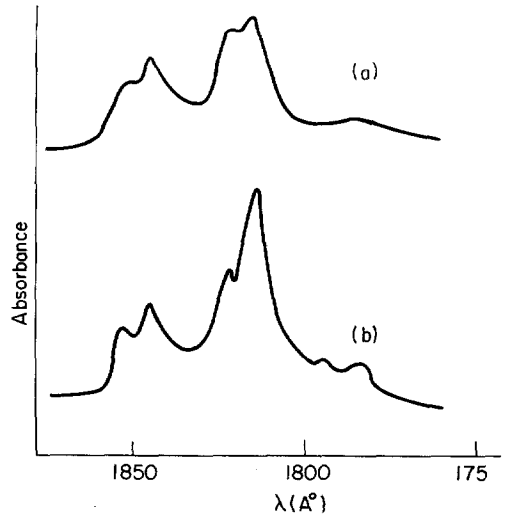

FIG. 5. The $^1A_{1g}\rightarrow{}^1E_{1u}$ transition of C_6D_6 in Kr (uncorrected microdensitometer tracings). Upper curve: deposition and measurement at 20°K. Lower curve: deposition and measurement at 4°K.

finally the vibronic wavefunctions are displayed in the form

$$\psi_p(\mathbf{q},\mathbf{Q})=\sum_{\alpha=m,n}\sum_i C_{\alpha i}{}^p\psi_\alpha{}^0(\mathbf{q},\mathbf{Q}_0)N_i(\mathbf{Q}). \quad (6)$$

The molecular Hamiltonian is now expanded in a Taylor series in the ground-state nuclear normal coordinates about the configuration $\mathbf{Q}_0$,

$$H(\mathbf{q},\mathbf{Q})=T_e(\mathbf{q})+T_N(\mathbf{Q})+U(\mathbf{q},\mathbf{Q}_0)+\sum_L[\partial U(\mathbf{q},\mathbf{Q})/\partial Q_L]_0Q_L+\tfrac{1}{2}\sum_L\sum_{L'}[\partial^2U(\mathbf{q},\mathbf{Q})/\partial Q_L\partial Q_{L'}]_0Q_LQ_{L'}. \quad (7)$$

In the calculation of the matrix elements of the molecular Hamiltonian (7) in the basis set $\psi_\alpha{}^0(\mathbf{q},\mathbf{Q}_0)N_i(\mathbf{Q})$ the off-diagonal matrix elements of the linear coupling terms are of crucial importance; those are given in the form

$$\langle\psi_n{}^0(\mathbf{q},\mathbf{Q}_0)\prod_J v_J\,|\times\sum_L[\partial U(\mathbf{q},\mathbf{Q})/\partial Q_L]_0Q_L\,|\,\psi_m{}^0(\mathbf{q},\mathbf{Q}_0)\prod_J v_J'\rangle=\sum_L K_{nm}{}^L[(v_L+1)^{1/2}\delta(v_L+1,v_L')+(v_L)^{1/2}\delta(v_L-1,v_L')]\otimes\prod_{J\neq L}\delta(v_J,v_J'). \quad (8)$$

The vibronic coupling matrix elements are

$$K_{nm}{}^L=\langle\psi_n{}^0(\mathbf{q},\mathbf{Q}_0)\,|\,[\partial U(\mathbf{q},\mathbf{Q})/\partial Q_L]_0\,|\,\psi_m{}^0(\mathbf{q},\mathbf{Q}_0)\rangle\otimes\langle 0_L\,|\,Q_L\,|\,1_L\rangle. \quad (9)$$

The molecular Hamiltonian (7) can now be (8) diagonalized in the representation $\psi_\alpha{}^0(\mathbf{q},\mathbf{Q}_0)N_i(\mathbf{Q})$. This procedure results in the vibronic energy levels. The intensity ratios can be readily evaluated from the mixing coefficients $C_{\alpha i}{}^p$. Sharf *et al.*[52] have performed detailed calculations on the pseudo-Jahn–Teller coupling between the $^1E_{1u}$ and the $^1B_{1u}$ states of the benzene molecule. The gross features of the theoretical results can be obtained when one retains diagonal matrix elements of the zero-order Hamiltonian $T_e(\mathbf{q})+T_N(\mathbf{Q})+U(\mathbf{q},\mathbf{Q}_0)+\frac{1}{2}\sum_L(\partial^2U/\partial Q_L{}^2)_0Q_L{}^2$ and off-diagonal linear terms in nuclear displacements [Eq. (8)]. For simplicity the changes in the vibrational frequencies in the excited electronic states relative to the ground state were disregarded. The electronic energy gap between the two electronic levels is 5600 cm^{-1}. The $^1B_{1u}$ and the $^1E_{1u}$ states are mixed by four vibrations of e_{2g} symmetry. These calculations have been carried out by Sharf and Honig who have considered the three $\nu_{18}(e_{2g})=606$ cm^{-1}, $\nu_{17}(e_{2g})=1174$ cm^{-1}, and $\nu_{16}(e_{2g})=1596$ cm^{-1} vibrations (where ground-state frequencies will now be applied) and neglected the effect of the $\nu_{15}(e_{2g})=3043$ cm^{-1} C–H stretching vibration. The calculations were performed taking a basis set of 31 zero-order functions, where the computational procedure involves two iterations. Theoretical estimates of the vibronic coupling terms were taken from Albrecht's work.[31] Further calculations were performed using other values for the coupling parameters of the two-skeleton vibration, which do not differ by more than a factor of 2 from Albrechts estimates. These results are displayed in Table V where we have also included the results of the simple per-

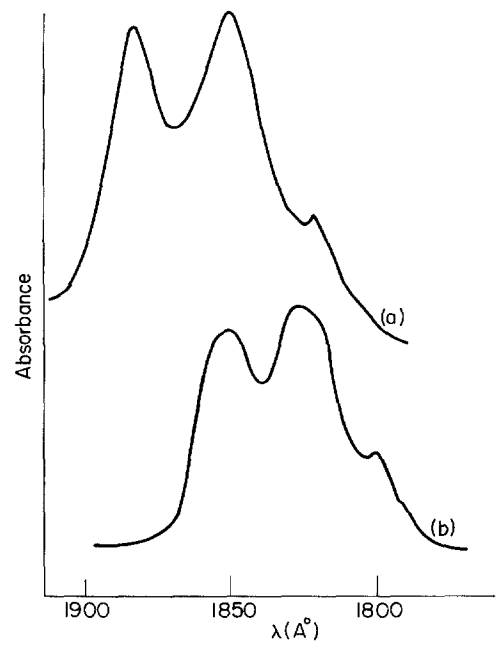

FIG. 6. The $^1A_{1g}\rightarrow{}^1E_{1u}$ transition of benzene in some inert matrices. Gas mixtures deposited and spectra measured at 20°K (uncorrected microdensitometer tracings). Upper curve: $C_3H_3D_3$/Xe. Lower curve: C_6D_6/N_2.

turbation treatment.[31] From these theoretical data we conclude that:

(a) Serious deviations from the results of simple perturbation treatment are encountered when relative level spacings are considered. The vibronic coupling effects between two closely lying states modify the relative location of the levels which correspond to the false vibrational origins. In particular it should be noted that the spacings between the false origins which correspond to $\nu_{18}(e_{2g})$ and the $\nu_{16}(e_{2g})$ vibrations is reduced.

(b) Dramatic effects are encountered when the relative intensities are considered. Second-order effects (which are, of course, omitted from the simple perturbation treatment) lead to transfer of intensity from the higher $\nu_{16}(e_{2g})$ strongly coupled component to the lower vibrational components.

(c) From these results we can conclude that a full-fledged variational treatment for vibronic interaction in the $^1B_{1u}$ state has to be performed and that the mutual effects of the several coupling vibrations have to be taken into account.[50,52]

(d) It is apparent that the predictions of the proper variational version of vibronic coupling theory based on theoretical estimates of the linear coupling terms are inadequate. The theoretical estimates of the K terms by Albrecht[31] when applied within the framework of the variational treatment predict that the $\nu_{17}(e_{2g}) = 1174$ cm^{-1} vibration should be observable and that the intensity of the $\nu_{18}(e_{2g}) = 606$ cm^{-1} false origin should exceed the intensity of the ν_1 $(e_{2g}) = 1600$ cm^{-1} origin by about a numerical factor of 4:1. Similar difficulties concerning the reliability of the K terms are encountered in the theoretical study of Jahn–Teller coupling in the Rydberg states of benzene where all theoretical calculations of the coupling matrix elements predicts that two progressions of the e_{2g} vibrations of frequencies of 606 and 1600 cm^{-1} should appear with about equal intensities.[52] The experimental data[33] reveal a single progression of a nontotally symmetric e_{2g} vibration of $\sim$600 cm^{-1}, which is assigned to $\nu_{18}(e_{2g})$, while the $\nu_{16}(e_{2g}) = 1600$ cm^{-1} vibration does not appear in the Rydberg spectrum so that the coupling terms corresponding to this vibration are small in that case. Turning our attention now back to the $^1B_{1u}$ state we are forced to conclude that the coupling term for the $\nu_{17}(e_{2g}) = 1174$ cm^{-1} vibration is appreciably smaller than that estimated from theory.

(e) When vibronic coupling matrix elements of reasonable magnitude are employed, taking K^{600} $(^1B_{1u}, {}^1E_{1u}) = 400$ cm^{-1} and K^{1600} $(^1B_{1u}, {}^1E_{1u}) = 800$ cm^{-1}, the spacing between the two false origins and their intensity ratio is in reasonable agreement with our experimental results for the 2100-Å transition.

(f) One should notice that when first-order perturbation theory is used[31] Albrecht's coupling parameters[31] provide reasonable agreement with the observed intensity data. However, this agreement must be considered as accidental in view of the dominating role of intravibrational interaction effects which have to be accounted for in terms of the variational scheme considered herein.

TABLE VI. Relative intensities in the $^1A_{1g} \rightarrow {}^1E_{1u}$ transition measured for C_6H_6 in annealed N_2.

ν (cm^{-1})	Relative intensity[a]	Assignment
53 880	1	0–0
54 810	2	0–0+$\nu_2(a_{1g})$
55 730	0.5	0–0+$2\nu_2(a_{1g})$

[a] Experimental accuracy: ±30%.

TABLE VII. Vapor matrix shifts for the first false origin of the $^1A_{1g} \rightarrow {}^1B_{1u}$ transition[a] in C_6H_6.

Matrix	Vapor matrix shift (cm^{-1})	Previous work[b] (cm^{-1})
Ar	−520	−1500
Kr	−780	•••
Xe	−1220	•••
N_2	−780	•••

[a] The gas-phase data are taken from the estimates of Potts (Ref. 22).
[b] Data of Roncin *et al.* (Ref. 23) for the shift of the center of gravity of the $^1A_{1g} \rightarrow {}^1B_{1u}$ transition in solid Ar.

VI. COMMENTS ON THE $^1B_{1u}$ ASSIGNMENT OF THE 2100-Å BAND

The assignment of the 2100 Å transition in benzene to the $^1A_{1g} \rightarrow {}^1B_{1u}$ transition is based on the observed vibrational structure. Although this criterion is sometimes referred to[55] as "weak" we believe that the combination of the experimental data with the theoretical arguments is rather conclusive. It will be useful at this point to consider related theoretical and experimental data which are relevant to this assignment. Our arguments pertaining to the symmetry of the 2100-Å band in benzene are supported by further experimental work on the optical spectra of methylated benzenes in rare-gas matrices carried out by us.[56] Utilization of the rare-gas hosts leads in some cases to much better spectral resolution than that reported by Potts[22] for these molecules in hydrocarbon glasses. In the methylated benzenes in view of the reduction in the molecular symmetry both the pure electronic and the vibronically induced components may be observed. On the basis of simple group theoretical arguments one can conclude that for C_{2v} symmetry (e.g., toluene) the 0–0 component is allowed for both states of the methylated

[55] J. R. Platt, J. Mol. Spectry. 9, 288 (1962).
[56] B. Katz, M. Brith, B. Sharf, and J. Jortner, "An Experimental Study of the Absorption Spectra of Benzene Derivatives in Rare Gas Solids" (unpublished).

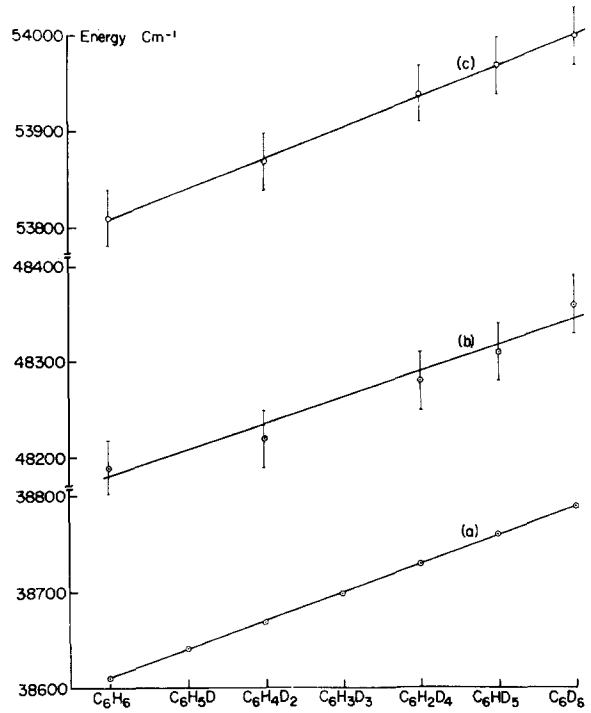

FIG. 7. Deuteration effects on the $\pi \rightarrow \pi^*$ transition energies in benzene. (a) The false origin of the $^1A_{1g} \rightarrow {}^1B_{2u}$ transition. Data from Ref. 7. (b) The lowest false origin of the $^1A_{1g} \rightarrow {}^1B_{1u}$ transition. (c) The 0–0 line of the $^1A_{1g} \rightarrow {}^1E_{1u}$ transition.

benzene having $^1E_{2g}$ and $^1B_{1u}$ parentage of the states of the benzene molecule. On the other hand, for the D_{2h} symmetry (e.g., *para*-xylene) the pure electronic transition is allowed only for the $^1B_{1u}$ state and forbidden for the $^1E_{2g}$ configuration. The 0–0 line was observed for *para*-xylene in rare-gas solids, these results concur with the data of Potts,[22] thus providing a strong supporting evidence for the $^1B_{1u}$ assignment. Further indirect support for the $^1B_{1u}$ assignment arises from Petruska's work[57] on the patterns of shifts of the center of gravity of the 2100-Å band upon chemical substitution. It should, however, be pointed out that these calculations considered only the changes in electronic energies while vibronic effects were not included. From the studies of the pseudo-Jahn–Teller effect in the negative ions of substituted benzenes it is known that the vibronic effects seriously modify the energy levels.[41]

The different criteria for the identification of the 2100-Å symmetry-forbidden spin-allowed transition can be summarized as follows:

(a) Current energy-levels calculations are in disagreement with the $^1B_{1u}$ assignment.[27–29] Reassessment of the adequacy of CI SCF π-electron calculations (even when double and higher excitations are included) is still required.

(b) Agreement with the calculated absorption intensity is not conclusive in the present case, oscillator strengths in the region 0.05–0.1 are predicted both for the $^1E_{2g}$ and for the $^1B_{1u}$ excitation.[30,31] The application of the variational method[53] outlined in Sec. IV does not modify these results.

(c) The vibrational structure is consistent with the $^1B_{1u}$ assignment.

(d) "Symmetry breaking" effects resulting in the reduction of molecular symmetry support the $^1B_{1u}$ assignment.[22,56]

(e) Spectral shifts support again the $^1B_{1u}$ assignment,[57] although further theoretical work on this subject including vibronic coupling effects is still required.

To conclude this discussion we should consider briefly the results of a recent study on high-resolution electron-impact spectroscopy of benzene performed by Lassettre *et al.*[58] Four vibronic components were reported in the region 6.20–6.53 eV with a spacing of $\sim$900 cm^{-1}. A fifth weaker component located at about 6.10 eV seems to appear as a shoulder (see Figs. 15 and 19, Ref. 58). Thus the general appearance of the electron-impact spectrum as far as the intensity pattern and the level spacing are concerned is similar to the matrix spectra reported herein. However, the electron-impact spectra studied at different scattering angles[58] indicate that the peak at 6.20 eV and presumably also the shoulder at 6.10 eV may correspond to a different electronic transition than the last three vibronic compounds. Our matrix data cannot resolve this problem, although the observed intensity pattern seems to support the assignment of the vibrational components to a single electronic state (see also Sec. X). Further theoretical work on the angular dependence of electron–molecule scattering is required.

VII. THE 1850-Å TRANSITION

The third singlet $\pi \rightarrow \pi^*$ transition of the benzene molecule is conventionally assigned to the $^1E_{1u}$ state.[1] In the gas phase this transition overlaps the $2R$ Rydberg level.[33] It was reported by Potts[22] that the vibrational structure of this $\pi \rightarrow \pi^*$ transition can be resolved in a hydrocarbon glass. Similar and even somewhat more pronounced features of the 1850-Å transition are observed in inert matrices as evident from Figs. 4–6. The $\pi \rightarrow \pi^*$ transition is separated from the Rydberg transition in the matrix in view of the different matrix shifts of these two states. While the $^1A_{1g} \rightarrow {}^1E_{1u}$ $\pi \rightarrow \pi^*$ transition is red shifted in the matrix the $^1A_{1g} \rightarrow 2R$ excitation undergoes an appreciable blue shift in rare-gas solids.[24,59] A detailed study of the Rydberg states of benzene in rare-gas solids has been performed by us,[59] and we have demonstrated that the Rydberg states (or rather Wannier states) of organic molecules are

[57] J. Petruska, J. Chem. Phys. **34**, 1120 (1961).

[58] E. N. Lassetre, A. Skerbele, M. A. Dillon, and K. J. Ross, J. Chem. Phys. **48**, 5066 (1968).

[59] B. Katz, M. Brith, B. Sharf, and J. Jortner, J. Chem. Phys. **50**, 5195 (1969).

amenable to experimental observation in the rare-gas solids. These Rydberg-type levels are appreciably blue shifted; however, line broadening in the rare-gas matrix is not excessive.

The $^1A_{1g} \rightarrow {}^1E_{1u}$ transition in the inert matrices reveals the following features:

(a) The fine structure of the vibronic components is attributed again to site splittings. From Figs. 4 and 5 it is apparent that high-temperature deposition of C_6H_6/Kr greatly reduced this fine structure while in C_6D_6/Kr this fine structure still persists even at higher deposition temperatures. It should be pointed out that in our previous communication[24] we have attempted to assign the broadening of the second line in the progression observed in an annealed C_6H_6/Kr sample (Fig. 4) to predissociation; however, our complete data (see, for example, the N_2 results in Fig. 6) do not support this conclusion.

(b) From the features of the vibrational structure displayed in Table III, it is apparent that a progression of five lines is observed with spacing of 920 ± 50 cm^{-1} in C_6H_6 and 850 ± 50 cm^{-1} in C_6D_6. The vibronic structure is consistent with a a_{1g} vibration.

(c) The intensity pattern of the vibrational components (Table VI) is not inconsistent with a single totally symmetric progression.

(d) No experimental evidence has been obtained for a nontotally symmetric e_{2g} vibration which might have been induced by Jahn–Teller interactions in the $^1E_{1u}$ state. This negative result is consistent with the predictions of first-order theory whereupon there are no Jahn–Teller coupling effects for the electronic configuration $(a_{2u})^2(e_{1g})^3(e_{2u})^1$, as accidental cancellation of the vibronic coupling terms should occur. This problem will now be briefly considered.

VIII. JAHN–TELLER COUPLING IN THE $^1E_{1u}$ STATE

We shall now demonstrate that no Jahn–Teller coupling effects are expected to be exhibited in the $^1E_{1u}$ $\pi \rightarrow \pi^*$ excited state when single configuration electronic wavefunctions are employed. This is due to the fact that the two degenerate components differ in the occupation of two molecular orbitals and thus cannot be coupled by one-electron perturbation. This argument is not new[52]; however, it would be useful to recast it in a more transparent form. The first-order electronic wavefunction of the $^1E_{1u}$ state can be displayed in the LCAO electron approximation[60]

$$\psi_\alpha = (1/\sqrt{2})(\phi^{3\rightarrow 5} + \phi^{2\rightarrow 4}),$$
$$\psi_\beta = (1/\sqrt{2})(\phi^{3\rightarrow 4} - \phi^{2\rightarrow 5}), \qquad (10)$$

where $\phi^{i\rightarrow j}$ describes an excitation from the MOμ_i to the MOμ_j, and we have used the conventional notation

[60] See any quantum chemistry text.

TABLE VIII. Vapor matrix shifts for the 0–0 $^1A_{1g} \rightarrow {}^1E_{1u}$ transition[a] in C_6H_6.

Matrix	Vapor matrix shift (present work) (cm^{-1})	Previous[b] results (cm^{-1})
Ar	−1130	−1200
Kr	−1610	•••
Xe	−2350	•••
N_2	−1540	•••

[a] The 0–0 line in the gas phase is taken from Wilkinson's work (Ref. 33).
[b] The shift of the center of gravity of the $^1A_{1g} \rightarrow {}^1E_{1u}$ transition in Ar was reported by Roncin *et al.* (Ref. 23).

for the π electron MO's of benzene in their real representations. The formulation of the electronic–vibrational coupling is straightforward. Applying the crude adiabatic approximation[42] (see also Sec. V) the relevant vibronic wavefunctions are

$$\psi_p(\mathbf{q}, \mathbf{Q}) = \chi_{p\alpha}(\mathbf{Q})\psi_\alpha(\mathbf{q}) + \chi_{p\beta}(\mathbf{Q})\psi_\beta(\mathbf{q}). \qquad (10')$$

The expansion coefficients $\chi_{p\alpha}(\mathbf{Q})$ and $\chi_{p\beta}(\mathbf{Q})$ can be again expanded in terms of products of harmonic-oscillator nuclear functions. Consider a single doubly degenerate e_{2g} frequency which couples the electronic states. Let Q_a and Q_b correspond to the (real) normal coordinates of this vibration. When linear coupling terms are retained the relevant electronic matrix elements are of the form

$$K_{\alpha\alpha}{}^a = \langle \psi_\alpha \mid (\partial U/\partial Q_a)_0 \mid \psi_\alpha \rangle,$$
$$K_{\beta\beta}{}^a = \langle \psi_\beta \mid (\partial U/\partial Q_a)_0 \mid \psi_\beta \rangle,$$
$$K_{\alpha\beta}{}^b = \langle \psi_\alpha \mid (\partial U/\partial Q_b)_0 \mid \psi_\beta \rangle. \qquad (11)$$

Bearing in mind that $(\partial U/\partial Q_i)_0$ involves only one-electron operators we can immediately reduce coupling terms into one-electron integrals:

$$K_{\alpha\alpha}{}^a = \langle \mu_5 \mid (\partial U/\partial Q_a)_0 \mid \mu_5 \rangle + \langle \mu_4 \mid (\partial U/\partial Q_a)_0 \mid \mu_4 \rangle - \langle \mu_3 \mid (\partial U/\partial Q_a)_0 \mid \mu_3 \rangle - \langle \mu_2 \mid (\partial U/\partial Q_a)_0 \mid \mu_2 \rangle,$$
$$K_{\beta\beta}{}^a = K_{\alpha\alpha}{}^a,$$
$$K_{\alpha\beta}{}^b = \langle \mu_2 \mid (\partial U/\partial Q_b)_0 \mid \mu_3 \rangle - \langle \mu_2 \mid (\partial U/\partial Q_b)_0 \mid \mu_3 \rangle + \langle \mu_4 \mid (\partial U/\partial Q_b)_0 \mid \mu_5 \rangle - \langle \mu_4 \mid (\partial U/\partial Q_b)_0 \mid \mu_5 \rangle. \qquad (12)$$

Using the relations

$$\langle \mu_2 \mid (\partial U/\partial Q_a)_0 \mid \mu_2 \rangle = -\langle \mu_3 \mid (\partial U/\partial Q_a)_0 \mid u_3 \rangle$$

and

$$\langle \mu_4 \mid (\partial U/\partial Q_a)_0 \mid \mu_4 \rangle = -\langle \mu_5 \mid (\partial U/\partial Q_a)_0 \mid \mu_5 \rangle$$

it is immediately apparent that for this state $K_{\alpha\alpha}{}^a = K_{\beta\beta}{}^a = 0$, and of course $K_{\alpha\beta}{}^b = 0$, so that linear coupling terms vanish. The same treatment can be extended for off-diagonal quadratic coupling terms. It should be borne in mind that this argument rests on the application of a single-configuration wavefunction; although

the inclusion of configuration interaction[25–29] is expected to lead to nonvanishing linear (and quadratic) terms in nuclear displacements, the resulting coupling terms are expected to be small relative to the frequency of the vibrations which couples the degenerate levels, and Jahn–Teller coupling effects will not be manifested in the optical spectrum for this transition.

IX. ISOTOPE EFFECTS

It is well known that upon deuteration the false origin of the $^1A_{1g}\rightarrow{}^1B_{2u}$ transition is blue shifted by 30 cm^{-1} per deuterium atom, while the shift of the forbidden 0–0 line for this transition is 33 cm^{-1} per D atom.[7,61] The origin of this shift is attributed to the fact that while there is practically no change in the electronic energy the zero-point vibrational energies of both states are reduced upon deuteration, while the zero-point nuclear energy is lower in the excited $^1B_{2u}$ state than in the ground state. The deuterium isotope effects on the higher $\pi\rightarrow\pi^*$ transitions are summarized in Fig. 7 where we have displayed the first false origin of the $^1A_{1g}\rightarrow{}^1B_{1u}$ transition and the 0–0 band of the $^1A_{1g}\rightarrow{}^1E_{1u}$ excitation. The isotope shifts from C_6H_6 to C_6D_6 are 150 ± 50 cm^{-1} for the $^1B_{1u}$ state and 190 ± 50 cm^{-1} for the $^1E_{1u}$ state. Thus the isotope shifts per deuterium atom are 25 ± 8 cm^{-1} for the $^1A_{1g}\rightarrow{}^1B_{1u}$ first false origin and 31 ± 8 cm^{-1} for the pure electronic origin of the $^1A_{1g}\rightarrow{}^1E_{1u}$ excitation. We should note in passing that pseudo-Jahn–Teller coupling effects in the $^1B_{1u}$ state are not expected to seriously modify the observed isotope shift (within the large margin of the experimental uncertainty) as the vibronic coupling matrix elements for skeleton vibrations [Eq. (9)] are only weakly dependent on the isotopic compositions.[31] From these results we may conclude that the deuterium isotope effects on the second and third spin-allowed $\pi\rightarrow\pi^*$ excitation are very close to the effect observed on the lowest singlet state. This conclusion is not surprising as all these three excitations are constructed in first order from the same MO's, hence the charges in the force constants in the $^1B_{2u}$, $^1B_{1u}$, and $^1E_{1u}$ excited states relative to the ground state should be very close. Finally, we should point out that the frequencies of the a_{1g} vibrations in the $^1B_{1u}$ and in the $^1E_{1u}$ which are 920 ± 50 cm^{-1} for C_6H_6 and 850 ± 50 cm^{-1} for C_6D_6 for both states are consistent with the totally symmetric frequency[48] in the $^1B_{2u}$ state which is 923 cm^{-1} for C_6H_6 and 879 cm^{-1} for C_6D_6.

X. A COMMENT ON THE INTENSITIES OF VIBRATIONAL COMPONENTS

Approximate estimates of the Franck–Condon overlap integrals for the a_{1g} mode can be obtained by the Ross–McCoy[62] procedure and can be applied for the calculation of the relative intensities of the totally symmetric progression built on the false ($e_{2g}=1600$ cm^{-1}) origin in the $^1B_{1u}$ state and for the pure electronic origin in the $^1E_{1u}$ state. The relative intensity of the nth vibrational component relative to the zeroth totally symmetric component is given by McCoy and Ross in the form[62]

$$I_n/I_0=(x^{2n}/n!)\,(E_n/E_0),$$

where E_n ($n=0, 1, \cdots$) correspond to the energies, while the parameter x is determined by the force constant, the vibrational frequency, and by an effective length representing the displacement of the origin of the configuration coordinate for the a_{1g} vibration. The calculations of McCoy and Ross on the benzene molecule[62] lead to the following results: $x=1.19$ for the $^1B_{2u}$ state, $x=0.84$ for $^1B_{1u}$ level, and $x=1.0$ for the $^1E_{1u}$ configuration.

Hence the intensity pattern in the $^1A_{1g}\rightarrow{}^1B_{1u}$ transition is expected to be (taking the intensity of the false $\nu_{16}(e_{2g})\approx1600$ cm^{-1} origin as unity) 1:0.7:0.25:0.10. The experimental intensity data (Table V) are 1:0.80:0.50:0.22. These results clearly indicate that the lowest vibronic component observed experimentally in the $^1A_{1g}\rightarrow{}^1B_{1u}$ transition cannot be assigned to the same vibrational progression. The agreement between theory and experiment is reasonable and a slight change of the x parameter from $x=0.84$ to $x=1.0$ will lead to good agreement with experiment.

The intensity pattern in the $^1A_{1g}\rightarrow{}^1E_{1u}$ transition predicted by McCoy and Ross (taking the intensity of the 0–0 component as unity) is: 1:1:0.5:0.17; this compares reasonably with the experimental data (Table VII) 1:2:0.5:$\sim$0.1, providing a proper interpretation for the rapid falloff in the intensity of the higher vibrational components for this transition. We do not understand the reason for the higher relative intensity of the second component in this state, although the existence of an overlapping "hidden" transition can always be blamed for the discrepancy between theory and experiment.

XI. REMARKS ON MATRIX SHIFTS

The present study provides some further information on the matrix effects on the excitation energies of a polyatomic molecule in molecular solids. In Tables VII and VIII we have summarized these results for the first false vibronic origin of the $^1A_{1g}\rightarrow{}^1B_{1u}$ transition (which is located in the gas phase at 48 970 cm^{-1}) and for the 0–0 line of the $^1A_{1g}\rightarrow{}^1E_{1u}$ transition (which was identified in the gas phase at 55 420 cm^{-1}). The present results are compared with the data of Roncin *et al.*[23] for the matrix shifts of the center of gravity of the electronic transitions in solid Ar. Our data are consistent with the approximate theory of Longuet-Higgins and Pople,[63] who displayed the solvent shift δ in

[61] F. M. Crawford, C. K. Ingold, and H. G. Poole, J. Chem. Soc. **1948**, 508.

[62] E. McCoy and I. G. Ross, Australian J. Chem. **15**, 573 (1962).

[63] H. C. Longuett-Higgins and J. A. Pople, J. Chem. Phys. **27**, 192 (1957).

the form $\delta = -\alpha_M R^{-6}(\frac{1}{4}E\alpha_B + M^2)/6$, where α_M and α_B are the polarizabilities of the matrix atom and of the impurity molecule, respectively, R is a mean guest–host spacing, while M corresponds to the transition moment. The application of this result for the second and third spin-allowed excitation in benzene leads to the following result for the relative shifts for these two transitions in the same matrix: $\delta(^1A_{1g} \rightarrow {}^1E_{1u})/\delta(^1A_{1g} \rightarrow {}^1B_{1u}) = 2.3$. The experimental results are for these shifts ratios 2.2 for Ar, 2.1 for Kr, 1.9 for Xe, and 2.0 for N_2, in good agreement with the theoretical predictions. It should be recalled that matrix shifts for small atoms and for small molecules[64] in rare-gas solids cannot be accounted for in terms of such a simplified theory and short-range repulsions have also to be included.[64] It appears that for $\pi \rightarrow \pi^*$ excitation in a large molecule the role of dispersion interactions is dominating in determining the matrix shift.

XII. RADIATIONLESS TRANSITIONS AND LINE BROADENING

A phenomenon closely related to electronic relaxation in large molecules is the occurrence of line broadening in the absorption spectra of the higher excited electronic states.[10,11,13–15,64,65] In these excited states the Born–Oppenheimer separability conditions for electronic and nuclear motion break down because of vibronic coupling between isoenergetic zeroth-order Born–Oppenheimer vibronic states which correspond to different electronic configurations. In the statistical limit when the density ρ of vibronic levels (which correspond to the lower electronic states) is sufficiently high to exceed the reciprocal of the mean vibronic coupling term v between the zero states, inhomogenous line broadening is expected to be observed. For an isolated resonance, the line shape is expected to be Lorentzian,[10,65] and the line is given by $\Delta_i = 2\pi v^2 \rho$. Trivial causes for diffuseness in gas-phase spectra were studied in detail by Ross *et al.*[13–15] and these include mainly rotational structure and sequence spectral congestion. These causes are of course eliminated in solid matrices (hydrocarbons or solid rare gases); however, medium effects may be quite pronounced in certain cases. The matrix effects on the linewidths can be summarized as follows:

(a) Coupling of states with the lattice vibration of the host should lead to temperature-dependent broadening Δ_{ph} of all the vibronic levels for a given electronic state.

(b) Vibrational relaxation effects will lead to the broadening of the higher vibrational components within a given electronic state. These effects should be negligible for the 0–0 band, and an additional contribution to the line broadening over that of the 0–0 band gauges the vibrational relaxation process. This additional broadening due to vibrational relaxation[64] is in the range $\Delta_{vr} = 1$–10 cm^{-1}.

(c) In the statistical limit the radiationless relaxation times are expected to be independent of the medium.

Thus the total linewidth Δ of a large molecule in a solid can be displayed in the form $\Delta \approx \Delta_{ph} + \Delta_{vr} + \Delta_i$.

Turning our attention now to the electronic spectrum of benzene in the solids studied herein, we can infer that the $^1A_{1g} \rightarrow {}^1B_{1u}$ and $^1A_{1g} \rightarrow {}^1E_{1u}$ transitions are appreciably broadened in the low-temperature matrices. It is well known that the absorption spectra of the second excited singlet state of large molecules are broadened; however, quantitative data are lacking. To obtain some semiquantitative data, we note that the linewidths of C_6H_6 in Kr are: $\Delta(^1B_{2u}) \simeq 10$–$35$ cm^{-1} [66] for the $^1A_{1g} \rightarrow {}^1B_{2u}$ transition, $(^1B_{1u}) = 350$ cm^{-1} for the ν_{16} and ν_{18} false origins of the $^1A_{1g} \rightarrow {}^1B_{1u}$ transition, and $\Delta(^1E_{1u}) = 300$ cm^{-1} for the $^1A_{1g} \rightarrow {}^1E_{1u}$ transition. We may thus conclude that line broadening is severe in the two higher states relative to the lowest excited state. It should, however, be borne in mind that the Δ values given above provide us with an upper limit for line-broadening states as in the $^1B_{1u}$ and $^1E_{1u}$. Some contribution from site splittings may complicate the interpretation of the width.

From the available gas-phase data for the $^1A_{1g} \rightarrow {}^1B_{2u}$ transition we can ascertain that the effect of intramolecular electronic relaxation is negligible so that $\Delta_i \simeq 0$ and $\Delta(^1B_{2u}) = \Delta_{ph} + \Delta_{vr} \simeq 35$ cm^{-1}. We can further argue that the values of Δ_{ph} and of Δ_{vr} should not vary greatly between different $\pi \rightarrow \pi^*$ states arising from similar electronic configurations. This qualitative argument leads to the estimate for the line broadening arising from intramolecular radiationless decay, which is roughly $\Delta_i(^1B_{1u}) \simeq \Delta_i(^1E_{1u}) \simeq 300$ cm^{-1}. Hence the electronic relaxation times in the $^1B_{1u}$ and $^1E_{1u}$ excited states are of the order of $\hbar/\Delta_i \simeq 10^{-14}$ sec. It is unfortunately impossible to obtain quantitative information on the line shapes from the present data, as the photographic detection method is not reliable in this respect. Some interesting effects like deviations of the line shape from a Lorentzian shape[65] and interference between overlapping resonances[65] are expected to be observed; however, our experimental data are not sufficiently accurate for such a detailed analysis.

On the basis of the semiquantitative data presented above we can infer that intramolecular electronic relaxation is extremely efficient in the second singlet excited state of the benzene molecule which is located about 10 000 cm^{-1} above the first excited singlet. The general appearance of the diffuseness in the second excited singlet state of benzene is radically different

[64] R. M. Hochstrasser, Acct. Chem. Res. **1**, 266 (1968).
[65] D. Chock, J. Jortner, and S. A. Rice, J. Chem. Phys. **49**, 610 (1968).

[66] This result for the $^1B_{2u}$ may be an overestimate, as the spectral resolution is $\lesssim 10$ cm^{-1}, so that instrumental broadening may be encountered.

from the behavior of the second excited singlet of the naphthalene molecule,[67,68] where the energy gap between the first and second singlet states is 3000 cm^{-1}. In the case of the naphthalene molecule a careful study of the second singlet state in a mixed crystal reveals a number of relatively sharp lines superimposed on a diffuse background.[67,68] These are attributed to zero-order vibrational levels of the lower singlet state which borrow intensity by pseudo-Jahn–Teller coupling from the (zero-order) second singlet state. These features are not observed for the second singlet of benzene. From this comparison we can conclude that line broadening in higher excited singlet states depends strongly on the energy separation between the excited states. Furthermore, vibronic interference effects can be observed only when the energy gap is relatively small.

[67] D. S. McClure, J. Chem. Phys. **22**, 1968 (1954).
[68] D. S. McClure and J. Wessel (private communication).

ACKNOWLEDGMENTS

We are indebted to Dr. Barry Honig for many helpful discussions and for his help in the theoretical calculations. We wish to thank Dr. Arza Ron for helpful discussions. We are grateful to the Department of Chemistry, The Technion, Haifa, for the use of their vacuum spectrograph.

THE JOURNAL OF CHEMICAL PHYSICS VOLUME 52, NUMBER 1 1 JANUARY 1970

Second-Order Perturbation Treatment of the Ground State of H_2^+

M. JACKSON AND R. P. MCEACHRAN
Centre for Research in Experimental Space Science and Department of Physics, York University, Toronto, Canada
AND
M. COHEN
*Centre for Research in Experimental Space Science and Department of Physical Chemistry, The Hebrew University, Jerusalem, Israel**

(Received 14 August 1969)

Rayleigh–Schrödinger perturbation theory has been used through second order to obtain an analytic representation for the ground-state wavefunction of H_2^+. Values of the electronic energy and other molecular properties computed with this approximate wavefunction are compared with the corresponding exact values, and they demonstrate its high accuracy.

I. INTRODUCTION

The hydrogen-molecule ion occupies a central position in theories of molecular structure, similar to that of the hydrogen atom in atomic theory. As such, it has attracted a considerable amount of attention from theorists, from the early work of Burrau[1] to the most recent and very accurate calculations of Bates, Ledsham, and Stewart,[2] Hunter and Pritchard,[3] Wind,[4] and Peek.[5]

Despite the availability of these highly reliable wavefunctions, there has been considerable interest in approximate representations, particularly for the ground ($1s\sigma_g$) state of the ion. Most of these functions have been derived variationally, and they have often yielded total electronic energies of fair accuracy over a limited range of internuclear separations. Molecular properties other than the electronic energy were compared by Dalgarno and Poots,[6] and their results showed clearly that approximate variational functions of "united-atom" type are likely to be more reliable than their "separated-atom" counterparts over a wide range of internuclear separations.

Recently, there have been a number of attempts to improve the quality of simple variational functions by regarding them as zero-order approximations which may be systematically improved by means of conventional Rayleigh–Schrödinger perturbation theory.[7,8] In particular, Cohen and McEachran[7] have solved the first-order problem which arises from making the simplest possible zero-order choice (a united-atom function, with a single variable parameter), while Lyon *et al.*[8] have solved the (mathematically) more complicated first-order problem, based on the Guillemin–Zener[9] (two-parameter) wavefunction. The two treatments differ only in the choice of zero-order functions and yield results of similar (high) accuracy at small internuclear separations. At larger separations, the results of Lyon *et al.*[8] are more accurate, reflecting

* Permanent address.
[1] Ø. Burrau, Kgl. Danske Videnskab Selskab. Mat. Fys. Medd. **7**, No. 14 (1927).
[2] D. R. Bates, K. Ledsham, and A. L. Stewart, Phil. Trans. Roy. Soc. London **A246**, 215 (1953).
[3] G. Hunter and H. O. Pritchard, J. Chem. Phys. **46**, 2146 (1967).
[4] H. Wind, J. Chem. Phys. **42**, 2371 (1965).
[5] J. M. Peek, J. Chem. Phys. **43**, 3004 (1965).
[6] A. Dalgarno and G. Poots, Proc. Phys. Soc. (London) **A67**, 343 (1954).
[7] M. Cohen and R. P. McEachran, Can. J. Phys. **44**, 2809 (1966).
[8] W. D. Lyon, R. L. Matcha, W. A. Sanders, W. J. Meath, and J. O. Hirschfelder, J. Chem. Phys. **43**, 1095 (1965).
[9] V. Guillemin, Jr. and C. Zener, Proc. Natl. Acad. Sci. U.S. **15**, 314 (1929).